Modelling of phase noise from frequency references in bistatic radar

By Geoffrey M. Herbert
Radar and Electronic Warfare, QinetiQ, Malvern, UK

Abstract

Close to carrier phase noise in frequency sources is more problematic in bistatic than in monostatic radar systems. This is due to the absence of correlation between the transmitter and the receiver. One approach to alleviating this problem is to use atomic clocks rather than crystal oscillators for the stable frequency sources. This paper describes a method of modelling the phase noise in atomic frequency references based on a combination of standard power law models. The model parameters are selected to fit the time and frequency stability specifications, together with measured data obtained from radar receivers. The model is used to predict the performance degradation resulting from clock induced phase noise for various combinations of carrier frequency and integration time.

1. Introduction

A coherent pulse-Doppler radar estimates target range from the times at which scattered returns are received. Target radial velocity is estimated from the Doppler frequency calculated by measuring the difference in phase between returns from successive pulses. The transmit and receive platforms are separate in bistatic radars, whereas they are co-located in monostatic radars. Bistatic radar is described in Willis (1990). Bistatic radar systems have potential benefits over monostatic systems in a military context. Receive only platforms have more scope for covert operation than combined transmit/receive platforms. They can be positioned closer to hostile targets than transmitters can, without suffering an unacceptable risk of attack. They are also less vulnerable to targeted jamming. Synthetic aperture radar (SAR) systems combine returns received over long durations, e.g. tens of seconds, in order to generate high resolution ground maps. In addition to the general benefits of bistatic operation outlined above, bistatic geometries may facilitate improvements to imaging performance in some circumstances. Bistatic SAR is described in Horne & Yates (2002).

Stable frequency sources are required for satisfactory operation of a radar system in order to transmit at the required radio frequency (RF). They are also necessary in order to convert the received signals to a form which can be digitised and processed. Phase instability in the frequency sources results in distortion of the received signal, thereby causing errors in the estimation of target location and velocity. High frequency phase noise displaces the side-lobes of the Doppler spectrum corresponding to returns from a point scatterer. Low frequency phase noise distorts the central Doppler frequency. Phase noise at frequencies of the order of the reciprocal of the integration time can distort the shape of the Doppler spectrum around the central point.

Crystal oscillators can provide very good short term frequency stability. They are commonly used in monostatic radar systems. The low frequency phase noise is suppressed by the correlation between the transmitter and receiver when the same frequency source is used for both. Effective operation of bistatic systems is more complicated, as alignment in time and frequency (synchronisation and syntonisation) between the transmit and receive platforms is needed. If the platforms are in motion, as is the case with airborne radar systems, then continual updates to the navigation information providing the relative positions of the two systems are also needed. Crystal oscillators will often provide inadequate frequency stability, particularly at the long integration times associated with SAR applications. One option for alleviating this problem involves the use of a caesium or rubidium atomic frequency reference/clock on both platforms.

In order to predict the effects of clock induced phase noise on bistatic radar systems, it is necessary to estimate the phase noise as a function of frequency. The specifications of phase noise in atomic frequency references tend to cover frequencies above 1Hz, whereas values at lower frequencies are needed to ascertain the performance of radar systems with long integration times. Time domain stability specifications are given in the form of Allan deviations as described in Allan, Ashby & Hodge (1997). This paper describes a method of modelling the phase noise in atomic frequency references based on a combination of standard power law models for oscillator noise. The model parameters are estimated by fitting to the time and frequency stability specifications of the clocks, supplemented by measured data obtained from receivers.

Definitions of parameters used to measure time and frequency stability and the relationships between them are given in Section 2, together with consideration of the stability spectra corresponding to various types of noise. Section 3 deals with modelling the effects of phase noise from frequency references in a radar system. The principles underlying the operation of atomic frequency references are described in Section 4. Section 5 covers the construction of a model for

phase noise in the 5071A primary frequency standard with a high performance caesium tube (see Microsemi (2014)). Examples of the effects of the predicted phase noise on bistatic radar performance are given in Section 6, followed by the conclusions in Section 7.

2. Phase noise and Allan deviation

This section contains definitions of the parameters used to measure frequency and time stability, relationships between them and consideration of various types of noise. Much of the material is based on IEEE (2009) and Allan, Ashby & Hodge (1997).The phase of the output of a frequency reference as a function of time, $\Phi_{ref}(t)$, is given by

$$\Phi_{ref}(t) = 2\pi\nu_0 t + \phi(t), \tag{2.1}$$

where ν_0 is the reference frequency and $\phi(t)$ is the phase deviation of the signal. Amplitude deviation is assumed to be negligible in this paper. The characteristics of phase noise in a system are normally represented by the two sided spectral density function $\mathcal{L}(f)$, where $\phi_{rms}^2 = 2\int_0^\infty \mathcal{L}(f)df$, ϕ_{rms} is the root mean square value of $\phi(t)$ and f is the frequency offset relative to the carrier. This is normally expressed in units of dB below the carrier over a 1Hz bandwidth, dBc/Hz.

Phase instability can be expressed in units of time and frequency as $x(t) = \phi(t)/2\pi\nu_0$ and $y(t) = \frac{dx(t)}{dt}$. Instability of an oscillator in the time domain can be represented by the two-sample Allan deviation, $\sigma_y(\tau)$:

$$\sigma_y(\tau) = \left[\frac{1}{2}\langle[\bar{y}_{k+1} - \bar{y}_k]^2\rangle\right]^{1/2}, \tag{2.2}$$

where $t_k = t_0 + k\tau$, $\bar{y}_k = \frac{1}{\tau}\int_{t_k}^{t_{k+1}} y(t) = \big(x(t_{k+1}) - x(t_k)\big)/\tau$, t_0 is a time origin, k is an integer and $\langle\,\rangle$ denotes an infinite time average. This is expressed as a function of the interval between the two samples, τ. In practice it is estimated over a finite number of intervals.

The relationship between Allan deviation and phase noise spectral density is given in IEEE (2009):

$$\sigma_y^2 = \frac{4}{(\nu_0\pi\tau)^2}\int_0^{f_h} \mathcal{L}(f)\sin^4(\pi f t)df, \tag{2.3}$$

where f_h is the high frequency cut off for the applicable measurement system. It is shown by Greenall (1998) that inversion of this equation is not possible, and that there is not a unique mapping between Allan deviation and phase noise spectral density. A parametric inversion may be possible if assumptions are made about the spectrum.

Power law spectral densities are commonly used to model various types of random fluctuations in precision oscillators. The power laws corresponding to 'random walk frequency modulation' (FM), 'Flicker FM', 'White FM', 'Flicker phase modulation' (PM) and 'White PM' are given in Table 1. It is assumed that f_h has a high value and corresponds to an infinitely sharp low-pass filter. The terms for the five noise types can be summed if the random mechanisms are independent. A common model for phase noise in an oscillator has the form

Noise process	Spectral density, $\mathcal{L}(f)$	Allan deviation, $\sigma_y(\tau)$
Random walk FM	$k_{-4}f^{-4}$	$\sqrt{\frac{4k_{-4}\pi^2}{3\nu_0^2}}\tau^{1/2}$
Flicker FM	$k_{-3}f^{-3}$	$\sqrt{\frac{4k_{-3}\ln 2}{\nu_0^2}}$
White FM	$k_{-2}f^{-2}$	$\sqrt{\frac{k_{-2}}{\nu_0^2}}\tau^{-1/2}$
Flicker PM	$k_{-1}f^{-1}$	$\sqrt{\frac{k_{-1}(3\ln(2\pi f_h\tau) + 3\gamma - \ln 2)}{2\nu_0^2\pi^2}}\tau^{-1}$, where γ is the Euler-Mascheroni constant
White PM	k_0	$\sqrt{\frac{3k_0 f_h}{2\nu_0^2\pi^2}}\tau^{-1}$

TABLE 1. Power laws corresponding to noise types

$$\mathcal{L}(f) = k_0 + k_{-1}f^{-1} + k_{-2}f^{-2} + k_{-3}f^{-3} + k_{-4}f^{-4}, \tag{2.4}$$

where k_0, k_{-1}, k_{-2}, k_{-3} and k_{-4} are constant parameters specifying the level of each type of noise in the oscillator.

If $\phi(t)$ is small then a small angle approximation is applicable and the spectral density of the error in the output voltage of the oscillator resulting from the phase noise is approximately equal to that of $\mathcal{L}(f)$. The effect on the voltage spectral density of the total power in the $\mathcal{L}(f)$ spectrum going to ∞ as $f \to 0$ is considered by Chorti and Brookes (1991). It is assumed that the noise is a wide-sense stationary (WSS) process.

3. Modelling of phase noise in the radar system.

The output of the frequency reference is used to synthesise the local oscillator in the transmitter and receiver. A common output frequency for a reference source is 10MHz. Frequency multiplication is normally required, as the carrier frequencies of radar systems are often orders of magnitude higher. An ideal frequency multiplier operates as a phase multiplier. If the frequency is scaled by a factor of α then it follows from Equation (2.1) that the phase becomes

$$\Phi(t) = \alpha\big(2\pi\nu_0 t + \phi(t)\big). \tag{3.1}$$

The new nominal frequency is $\alpha\nu_0$, the new phase deviation is $\alpha\phi(t)$ and the new spectral density function of the phase noise is given by $\mathcal{L}(f) \to \alpha^2\mathcal{L}(f)$. If a local oscillator frequency of 10GHz is obtained from the 10MHz output of a frequency reference then the phase noise at all frequencies is increased by 60dB.

The signal at the receiver is digitised and down-converted. It is assumed that idealised generation of complex I and Q channels at baseband is performed. If a sinusoidal signal at the receiver with frequency ν_1 and amplitude A_1 is represented by $A_1 e^{i2\pi\nu_1 t}$ then the down-mixing process converts it to

$$s_1(t) = A_1 e^{i\left(2\pi(\nu_1 - \alpha\nu_0)t - \alpha\phi(t)\right)}. \tag{3.2}$$

If the transmitter is locked to the same local oscillator as the receiver, as is normally the case for a monostatic radar system, then there is correlation between the phase noise in the transmitted signal and in the signal used for down-mixing. In the ideal case in which the phase noise in the transmitted signal is identical to that in the receiver, the phase of the down-mixed output of the return from a point scatterer is approximately

$$\Phi_1(t) = 4\pi\alpha\nu_0 Vt/c + \alpha\left(\phi\left(t - \tfrac{2(r_0 - Vt)}{c}\right) - \phi(t)\right), \tag{3.3}$$

where V is the component of the relative velocity of the target towards the platform, r_0 is the target range at time $t = 0$ and c is the speed of propagation of electromagnetic radiation. This corresponds to a Doppler frequency of $2\alpha\nu_0 V/c$ and phase noise of $\alpha\left(\phi\left(t - \frac{2(r_0 - Vt)}{c}\right) - \phi(t)\right)$. If the change of target range over the integration time is assumed to be negligible, then it can be shown that the spectral density function of the phase noise at a frequency of f is scaled by a factor of $4\sin^2(2\pi f\, r_0/c)$. This is equivalent to the transmit-receive correlation factor described by Belcher & Morris (1993). The scale factor and corresponding reduction in phase noise increases with decreasing frequency. In a bistatic system, the phase noise on receive is independent of that on transmit and can be expressed as

$$\Phi_N(t) = \alpha_{tr}\phi_{tr}\left(t - \tfrac{2(r_0 - Vt)}{c}\right) - \alpha_{re}\phi_{re}(t), \tag{3.4}$$

where $(\alpha_{tr},\ \phi_{tr})$ and $(\alpha_{re},\ \phi_{re})$ are the values of α and ϕ corresponding to the transmitter and receiver respectively. Phase noise also results in timing errors of the order of $\phi(t)/2\pi\nu_0$. The effect of this on the Doppler spectrum is normally negligible compared with the effects described above.

Doppler processing is performed by applying a discrete Fourier transform (DFT) to time series data sampled at intervals of a pulse repetition interval (PRI). The Doppler spectrum corresponding to an ideal point target will depend upon the windowing function used and the target Doppler frequency relative to the centre of the nearest Doppler bin. Phase noise will distort the Doppler spectrum and degrade performance. Possible types of degradation include:

- Errors in the estimated target velocity resulting from displacement of the centre frequency.
- Reduction in target signal to noise ratio (SNR). This could be caused by a lowering of the peak Doppler response or an extended region of high side lobes.
- Poorer resolution of target velocities resulting from broadening of the Doppler main beam.
- False target detection due to high individual sidelobes. A target could appear at multiple Doppler frequencies.

Greenall (1998) states that 'in the range of frequencies the small-angle approximation is applicable, the oscillator power spectral density (PSD) coincides with the phase noise PSD'. Hence if Doppler main beam distortion caused by low frequency phase noise is negligible, the side-lobe levels as a function of frequency offset are approximated by

$$P(f) = \tfrac{\mathcal{L}_{co}(f)}{\tau_{int}} Q \sum_{p=1}^{Q} w_p^2 \big/ \big(\sum_{p=1}^{q} w_p\big)^2, \tag{3.5}$$

where τ_{int} is the integration time, w_p is element p of a windowing function of length Q and $\mathcal{L}_{co}(f)$ is the combined transmit and receive phase noise spectrum after frequency multiplication. The unambiguous extent of Doppler frequencies is equal to the pulse repetition frequency (PRF) and it follows that the actual side-lobe level at a particular frequency in this region will be approximated by the sum of the values given by Equation (3.5) for all of the equivalent aliased frequencies. Krieger & Younis (2006) state that the integrated side-lobe ratio (ISLR) may be approximated as ISLR $\approx 2\int_{1/\tau_{int}}^{\infty}\mathcal{L}_{co}(f)\,df$. If a windowing function were taken into account then the integration would start further out and a scale factor would be required as in Equation (3.5).

The main effect of phase noise at frequencies that are significantly lower than $1/\tau_{int}$ is to displace the central peak of the Doppler spectrum. The frequency error is given by $\frac{d\phi(t)}{dt}/2\pi$, which will not vary greatly over the integration time. The root mean square frequency offset resulting from phase noise between frequencies of f_1 and f_2 is given by

$$\Delta f_{rms}^2 = 2\int_{f_1}^{f_2} f^2\mathcal{L}_{co}df \tag{3.6}$$

if $f_1 < f_2 \ll 1/\tau_{int}$. Close to carrier phase noise at frequencies in the vicinity of $1/\tau_{int}$ causes distortion of the Doppler spectrum around the peak response. Simple formulae for predicting the behaviour of the Doppler spectrum in this region are not readily available, although some predictions are given by Krieger & Younis (2006).

4. Atomic clocks

The physical principles involved with the type of commercially available portable passive atomic clock that can be used as a frequency reference in a radar system are described by Lewis (1991), Bauch (2003) and Audoin & Vanier (1976). The energy difference between two quantum mechanical states of an atom is $h\nu_q$, where h is the Planck constant and ν_q is the frequency of electromagnetic radiation with photons of energy equal to this difference. The clock is prepared with atoms in one of these states, and microwave radiation is applied in order to cause a transition between states. The frequency is tuned to the value that produces the maximum number of transitions. For example, caesium clocks normally use a transition in the hyperfine structure of ^{133}Cs in the ground state with a frequency of $\nu_q = 9.192631770\text{GHz}$. The length of the second is defined in terms of this frequency. Rubidium vapour clocks use transitions in ^{87}Rb and ^{85}Rb.

The frequency output of the clock is normally that of a 5MHz or 10MHz crystal oscillator which is locked to the atomic transition frequency output and may be used to generate the signal applied to the atoms. The crystal oscillator has very good short term frequency stability. It follows that the phase noise spectral density is likely to correspond to that of the atomic reference at low frequencies and to the quartz oscillator at high frequencies. Cutler & Searle (1966) propose the following combination of the two frequency spectra:

$$\mathcal{L}_0(f) = \frac{f^n}{f^n+f_c^n}\mathcal{L}_{osc}(f) + \frac{f_c^n}{f^n+f_c^n}\mathcal{L}_{ref}(f), \tag{4.1}$$

where $\mathcal{L}_0(f)$ is the combined phase noise spectrum, $n = 2$, $\mathcal{L}_{osc}(f)$ refers to the phase noise in the crystal oscillator, $\mathcal{L}_{ref}(f)$ is the noise in the atomic reference and f_c is the loop cutoff for the oscillator and beam tube, which indicates the location of the transition between the two spectra.

Shot noise results from discrete movements or transitions that can be modelled as a Poisson process. It was first proposed in the context of fluctuations of current in vacuum tubes. The atomic signal depends upon the number of discrete transitions between the atomic states and hence shot noise is likely to dominate over a significant extent of frequency. Shot noise is equivalent to white FM and it therefore follows from table 1 that the phase noise spectrum will vary as $\mathcal{L}(f) \propto f^{-2}$ and the Allan deviation as $\sigma_y(\tau) \propto \tau^{-1/2}$ in this region. Lewis (1991) and Allan (1987) show typical Allan deviations as a function of time for various types of frequency reference. It can be seen that rubidium vapour clocks have short term stability that is comparable with caesium clocks. They are also significantly cheaper. Their long term stability is less good however. The Allan deviations flatten between 10^3 and 10^4 seconds and then start to rise with increasing time. The Allan deviations for typical caesium clocks do not flatten until around 10^5 to 10^6 seconds. The example of a quartz oscillator shown in Allan (1987) outperforms the atomic clocks at short times. Further examples of crystal oscillator spectra can be found in Ewell (1993).

5. Modelling of phase noise in atomic clocks

The frequency references were modelled as a combination of two oscillators as in Equation (4.1), with the option of increasing n above the default value of 2 in order to allow a sharper transition between the two regimes. The phase noise spectral density functions for the crystal oscillator and the atomic resonator were modelled as the sum of power laws corresponding to various types of noise as in Equation (2.4) i.e.

Offset (Hz)	$\mathcal{L}(f)$ at 10MHz output (dBc)	τ	$\sigma_y(t)$	τ	$\sigma_y(t)$
1	≤ -100	0.01s	$\leq 7.5\times10^{-11}$	10 000	$\leq 8.5\times10^{-14}$
10	≤ -130	0.1s	$\leq 1.2\times10^{-11}$	100 000	$\leq 2.7\times10^{-14}$
100	≤ -145	1s	$\leq 5.0\times10^{-12}$	5 days	$\leq 1.0\times10^{-14}$
1000	≤ -150	10s	$\leq 3.5\times10^{-12}$	30 days	$\leq 1.0\times10^{-14}$
10 000	≤ -154	100s	$\leq 8.5\times10^{-13}$	Guaranteed flicker floor	$\leq 1.0\times10^{-14}$
100 000	≤ -154	1 000s	$\leq 2.7\times10^{-13}$	Typical flicker floor	$\leq 5.0\times10^{-14}$

TABLE 2. Stability specifications of 5071A Primary frequency standard with high performance Caesium tube

$$\mathcal{L}_{osc}(f) = k_{0\_osc} + k_{-1\_osc}f^{-1} + k_{-2\_osc}f^{-2} + k_{-3\_osc}f^{-3} + k_{-4\_osc}f^{-4} \tag{5.1}$$

and

$$\mathcal{L}_{ref}(f) = k_{0\_ref} + k_{-1\_ref}f^{-1} + k_{-2\_ref}f^{-2} + k_{-3\_ref}f^{-3} + k_{-4\_ref}f^{-4}. \tag{5.2}$$

with an upper limit of f_h. The coefficients were set to zero unless otherwise stated.

This paper deals mainly with the case of a caesium 5071A primary frequency standard with a high performance tube on both the transmit and receive platforms. The stability specifications can be found in Microsemi (2014) and are reproduced in table 2. Phase noise spectral density values are given from 10^0 to 10^5Hz and Allan deviations are given from 0.01s to 30 days (2.592×10^6 seconds). In order to ascertain phase noise at frequencies below 1Hz and predict the performance of the bistatic radar system with long integration times, a model is constructed as described above and fitted to the specified Allan deviations and phase noise spectral density values.

Allan (1987) suggests that the typical noise types and ranges of applicability for a caesium resonator are white FM noise (>10s), flicker FM noise (> days) and random walk FM (> weeks). However, stability diagrams shown in Allan, Ashby & Hodge suggest that random walk FM noise in the 5071A may only become significant over a period of years rather than weeks. The noise from the Caesium tube in the 5071A was therefore initially modelled as a combination of white FM shot noise and flicker FM noise. The value of k_{-2_ref} was determined from the Allan deviation values between 100 and 100 000 seconds given in Table 2 and the formulae in Table 1. The value of k_{-3_ref} was based on the typical value of the flicker floor. It was found that the fit to the specified Allan deviation values could be improved by adding some flicker PM noise. Random-walk FM noise corresponding to environmental perturbations, which varies with f^{-4} will dominate at very low frequencies. This is negligible over the times for which the 5071A would be running in bistatic operations and has not been included in the model. Re-synchronisation and syntonisation of the references in the two systems would occasionally be required however.

Allan (1987) suggests that the typical noise types and ranges of applicability for a quartz oscillator are white PM noise (< 1ms), flicker PM noise (< 1s), flicker FM noise (> 1s) and random-walk FM noise (> h). White PM noise appears to be dominant at 10^5Hz in the specifications in Table 2 and the coefficient k_{0-osc} is determined from this value. Values for the k_{-1-osc} (flicker PM) and k_{-3-osc} (flicker FM) coefficients were chosen to attempt to fit the specified phase noise and Allan deviation values. Accurate estimation of k_{-4_osc} (random walk FM) from the specifications in table 2 is not possible or necessary, as the spectrum is determined by the atomic resonator at the relevant low frequencies. A value was chosen consistent with typical values given in Allan, Ashby & Hodge (1997), Diez, D'Angelo & Fernández (2006) and Shin, Park & Lee (2008). At low averaging times, the value of the Allan deviation is likely to depend upon the high frequency white PM phase noise. The high frequency cut off, f_h, was estimated from the values of $\sigma_y(t)$ at 10^{-2}s and $\mathcal{L}(f)$ at 10^5Hz. Accurate determination of this value is not critical

Coefficient	Based on specs	Based on specs and measurements	Coefficient	Based on specs	Based on specs and measurements
k_{0_ref}	0	0	k_{0_osc}	3.98×10^{-16}	3.98×10^{-16}
k_{-1_ref}	1.50×10^{-7}	5.25×10^{-8}	k_{-1_osc}	2.51×10^{-13}	2.51×10^{-13}
k_{-2_ref}	7.25×10^{-9}	1.82×10^{-9}	k_{-2_osc}	0	0
k_{-3_ref}	9.02×10^{-16}	9.02×10^{-16}	k_{-3_osc}	7.08×10^{-11}	7.08×10^{-11}
k_{-4_ref}	0	0	k_{-4_osc}	1.00×10^{-14}	1.00×10^{-14}
f_c	0.11	0.08	f_h	9.29×10^5	4.66×10^5
n	4	3			

TABLE 3. Model coefficients for 5071A with high performance tube

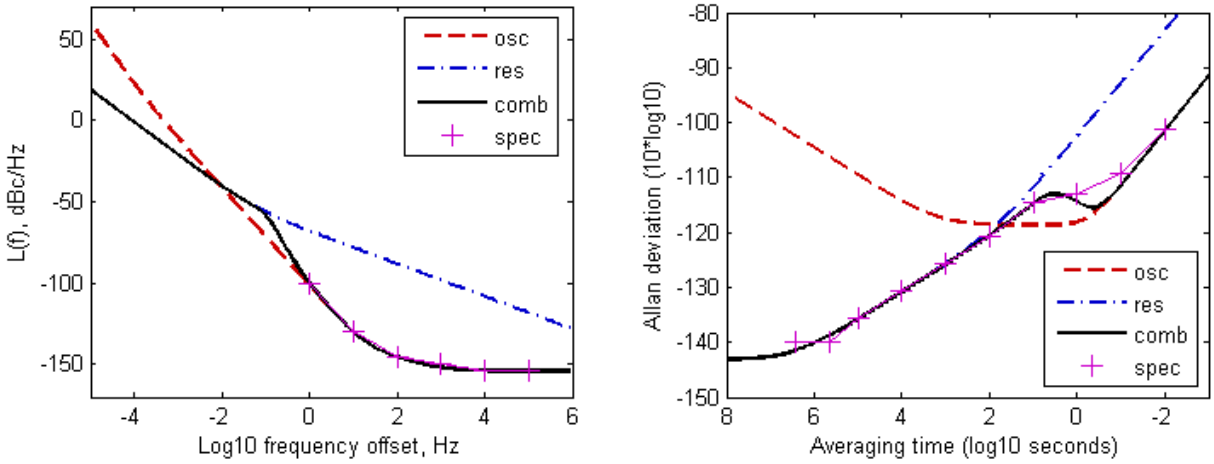

FIGURE 1. Modelled phase noise and Allan deviation for 5071A based on stability specifications.

however, as the close to carrier rather than the high frequency phase noise is of most significance for the bistatic radar performance.

The initial parameter estimates are shown in Table 3. The phase noise spectra and Allan deviation values corresponding to these values are shown in Figure 1. The plots show the modelled spectra for the crystal oscillator and the atomic resonator, together with the combined spectra and the values from the specification. Allan deviations were obtained by numerical integration of Equation (2.3) using the modelled phase noise spectra. The atomic resonator performs much better than the quartz oscillator at low frequencies and high averaging times as expected. At very high frequencies (above the cut off and not shown), the modelled resonator phase noise also falls below the modelled crystal oscillator noise. This would not be significant if it occurred below the cut off however, as the modelled oscillator spectrum also includes noise from the electronics and amplification of the clock, from which the output of the atomic resonator cannot be separated. The combined spectrum follows the atomic resonator spectrum at high frequencies/low averaging times and the crystal oscillator spectrum at high frequencies/low averaging times. The fit to the specified values of $\mathcal{L}(f)$ is good. The fit to the specified values of $\sigma_y(t)$ is reasonable, although the modelled values are 1-2dB below the specified values at averaging times of 1 and 10 seconds. The gradient of the combined Allan deviation curve changes sign for a short period in the transition region.

The values for phase noise spectral density and Allan deviation given in Microsemi (2014) and Table 2 are upper limits, apart from the typical value of the flicker floor, which is smaller than the guaranteed value by a factor of 2. Typical values at other frequencies could also be smaller.

The effects of phase noise of individual clocks on a radar system have been measured by injecting narrow-band signals into receivers locked to particular frequency references and then examining the resulting frequency spectra. If the side-lobes of a spectrum are dominated by oscillator induced phase noise then they should correspond to Equation (3.5) if the response around the central frequency is not distorted by close to carrier phase noise. An experiment has been performed using 5071a frequency references with high performance tubes. The integration time and carrier frequency were around 100s and 1GHz respectively. The side-lobe levels at a number of frequencies were estimated and compared with the values predicted by the model. It should be noted that there is a significant margin of error when estimating side-lobe levels from individual patterns. The estimated side-lobe levels at 1Hz were comparable with the predicted values. However, the predicted values at 0.1Hz were about 6dB higher than the estimated values. Results were also available for a combination of a 5071A and a Rubidium clock. The estimated side-lobes were similar from 0.1Hz outward, but the pattern showed more distortion at lower frequency offsets. This suggests that the transition between the crystal oscillator and atomic resonator may occur at a lower frequency than assumed in the model.

The model coefficients were adjusted in order to be more representative of typical clocks based on the above measurements. This process was somewhat speculative however. The adjusted model continued to fit to the phase noise specifications, but an additional phase noise value of -65.5dB was added at 0.1Hz based on the measured spectra described above. The Allan deviation values used to fit the model parameters were reduced by a factor of 2. This is consistent with the difference between the guaranteed and typical flicker floor values in Table 2. It can be seen from Equation (2.3) that it is also consistent with the 6dB overestimate of the side-lobe levels at 0.1Hz.

The model coefficients obtained when fitting to these revised values are shown in Table 3. The main changes are:

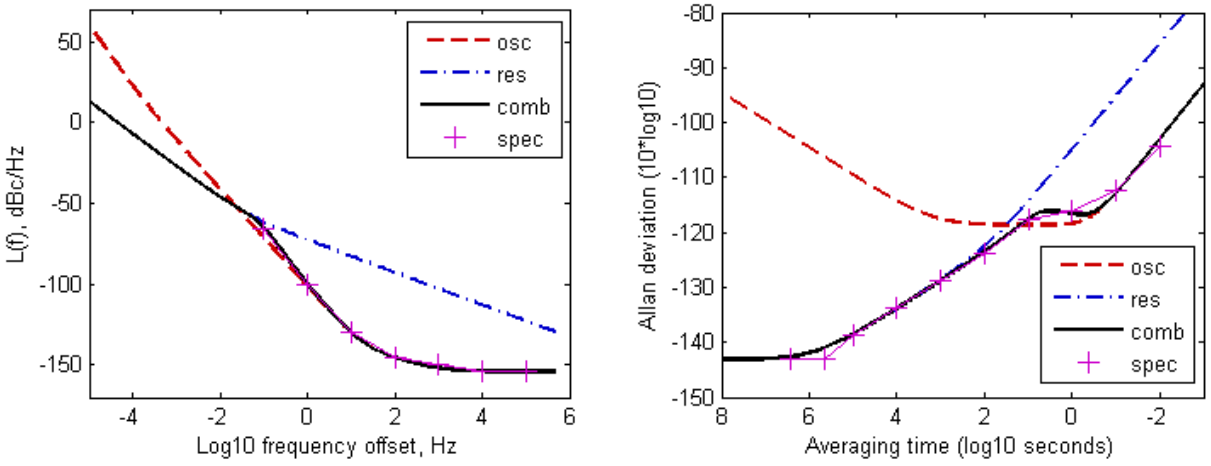

FIGURE 2. Modelled phase noise and Allan deviation for 5071A based on bistatic measurements.

- k_{-2_ref} and k_{-1_ref} are lower, corresponding to a reduction in the modelled phase noise for the atomic resonator.
- f_c and n are lower, resulting in a slightly wider transition region between the crystal oscillator and the atomic resonator that is centred at a lower frequency.

The resulting plots of phase noise PSD and Allan deviation are shown in Figure 2. The fit to the modified specifications looks reasonable, with a less pronounced gradient switch of the Allan deviation curve. It should be noted that the Allan deviations at short averaging times depend upon the high frequency cut off.

The phase noise spectral density and Allan deviation curves corresponding to the model before and after the adjustment are shown in Figure 3. The equivalent curve for a monostatic system with a target range of 100km and a crystal oscillator rather than an atomic clock is also shown. The same coefficients as for the crystal oscillator in the modified 5071A model were used to generate the monostatic results, together with correlation reduction as given in Equation (3.3). It can be seen that the low frequency phase noise for the ideal monostatic system is tens of dBs lower than for the bistatic system, even when atomic clocks are used.

6. Effect of modelled phase noise on radar performance

The effect of the modelled phase noise on the Doppler spectrum from a bistatic radar system corresponding to a narrow-band signal was simulated as follows: A set of frequency bins is specified covering the frequency extent of interest. A time series for the phase error for the clock to which the transmitter or receiver is locked is given by

$$\phi_s(t) = \sum_{k=1}^{n} 2\sqrt{\mathcal{L}_s(f_k)B_k}\cos(2\pi f_k t + \psi_k), \tag{6.1}$$

for $t = t_0, t_0 + \Delta t, \cdots t_0 + \tau_{int}$, where f_k is the central frequency of bin k, B_k is the size of bin k, s is the platform index (transmit or receive), ψ_k is a random phase between 0 and 2π at bin k, Δt is the sampling interval and τ_{int} is the

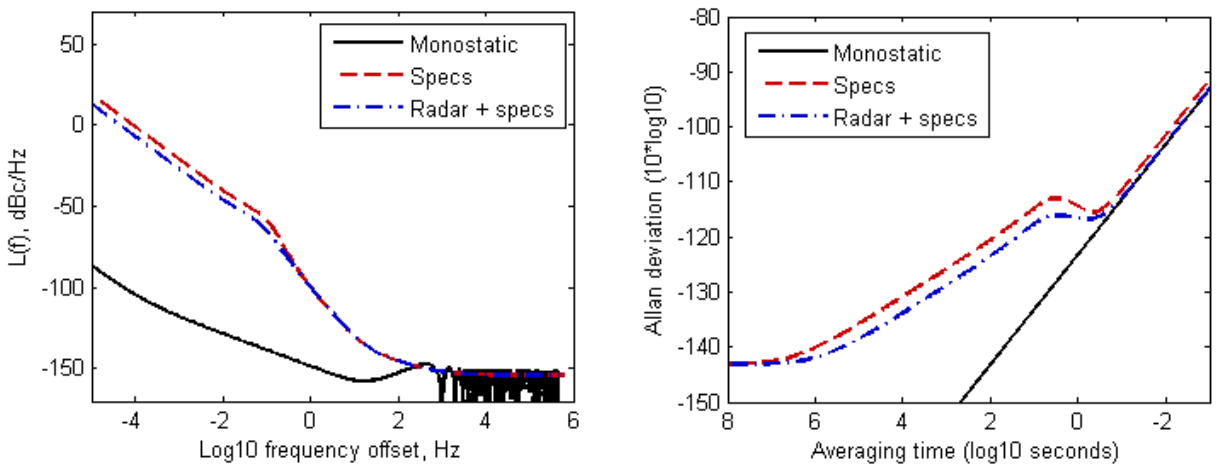

FIGURE 3. Comparison of 5071A model before and after modification and monostatic crystal oscillator model.

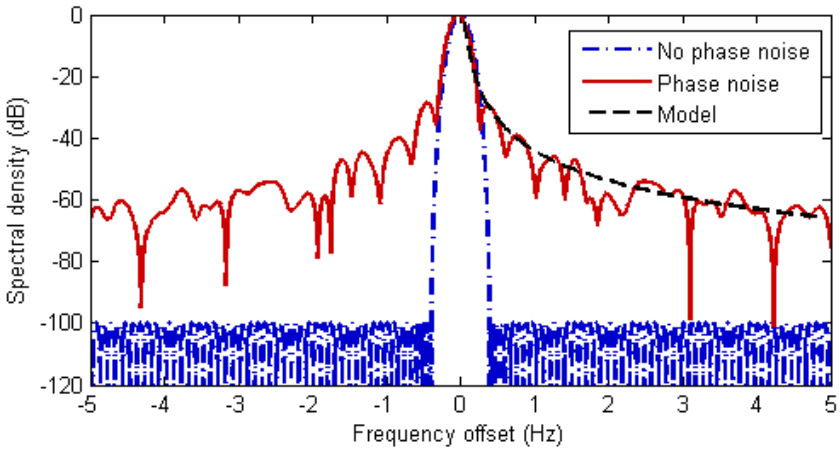

FIGURE 4. Effect of phase noise on radar performance with 5071A at 10GHz and 10s.

integration time. $\mathcal{L}_s(f_k)$ is the value of the phase noise spectral density function for the clock on platform s at bin k. The phase noise for the two platforms is then combined as in Equation (3.4) to determine the phase of the output time series. The time difference in Equation (3.4) can be excluded because of the randomisation in Equation (6.1). Note that in reality, the phase noise spectral density would have some random amplitude variation which is not included in the model.

An example Doppler spectrum simulated using a 5071a with a high performance tube on both the transmit and receive platforms is shown in Figure 4. The adjusted model was used with a carrier frequency of 10GHz and an integration time of 10s. The Fourier transform was performed with a 100dB Dolph-Chebyshev taper weighting function. Phase noise down to 10^{-6}Hz was simulated. The figure shows the spectra with and without the presence of clock induced phase noise noise, together with the side-lobe levels predicted by the model using Equation (3.5). The spectral density values are normalised to the peak level of the noise-free spectrum. There is a small amount of main-lobe distortion. The side-lobe levels are raised as expected and correspond reasonably well to the predicted curve.

The effects of phase noise become more severe with increasing frequency and integration time. A higher carrier frequency results in higher phase noise. A higher integration time corresponds to a narrower main-lobe. Errors in the central frequency are therefore proportionately larger. Main-lobe distortion results from phase noise at frequencies in the vicinity of $1/\tau_{int}$, and $\mathcal{L}(f)$ normally increases with decreasing frequency offset. An example Doppler spectrum at 20GHz and 20s is shown in Figure 5. There is noticeable displacement of the central frequency and considerable distortion of the main-lobe here. The spectrum corresponding to a monostatic scenario with a crystal oscillator with phase noise spectrum as shown in Figure 3 is also shown. The correlation between transmit and receive eliminates the main-lobe distortion.

Figure 6 shows the equivalent results with the integration time raised by another factor of 5 to 100 seconds. The main-lobe has been almost eradicated here, as the peak level is about 10dB down and is virtually indistinguishable from

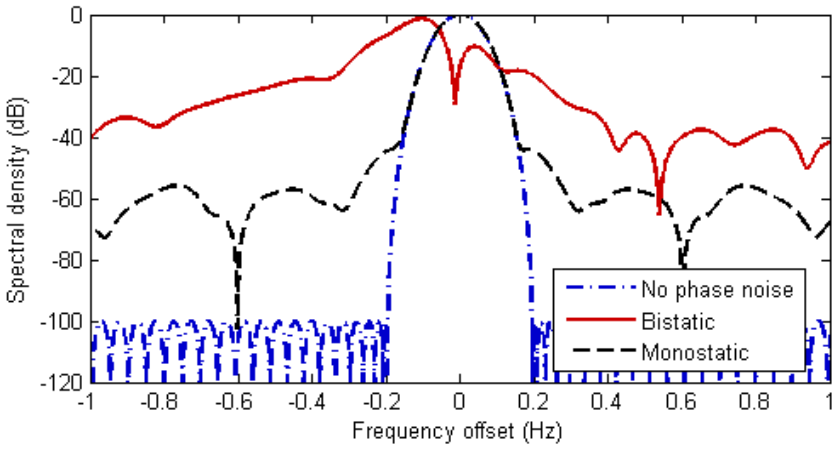

FIGURE 5. Effect of phase noise on radar performance with 5071A at 20GHz and 20s.

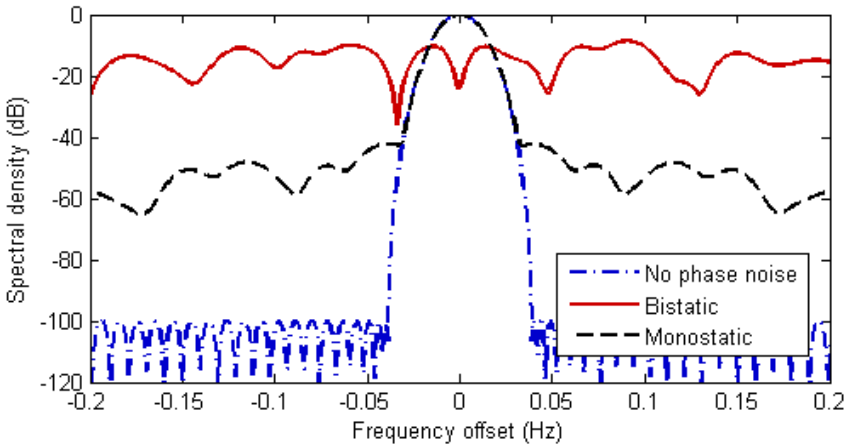

FIGURE 6. Effect of phase noise on radar performance with 5071A at 20GHz and 100s.

the near side-lobes. The main-lobe distortion is again negligible in the monostatic case.

The modelling process was repeated for a rubidium SA.22c-LN clock (specifications given in Symmetricom (2014)). Measured spectra corresponding to the SA.22c-LN showed larger frequency drifts than predicted by the model. This may be because Rubidium clocks are more susceptible than caesium clocks to frequency drift caused by environmental effects and processes other than random noise as described by Lewis (1991). They are also susceptible to aging. Allan, Ashby & Hodge state that systematic frequency drift occurs in crystal oscillators and rubidium frequency standards, and to a much lesser extent in caesium frequency standards. Long-time non-random processes are not represented by Allan deviations. An additional linear phase variation with time was incorporated into the model in order to account for this drift. Figure 7 shows example Doppler spectra at 20GHz carrier frequency and 20 seconds integration time for a pair of 5071a clocks with high performance tubes and a pair of SA.22c-LN clocks. The results for the rubidium pair are shown with and without the additional frequency drift. The random components of the noise coefficients in each frequency bin were the same in both cases. The shapes of the spectra are very similar. However, the SA.22c-LN spectrum shows over twice as much frequency drift as the 5071A even without the additional drift. This is because the modelled phase noise spectrum for the SA.22c-LN is similar to that of the 5071a at frequencies around $1/\tau_{int}$ and above, but higher at lower frequencies. The additional drift is much higher. More regular syntonisation would be needed to alleviate the effects of this drift.

It can be seen in Figure 2 that the 5071a model has higher phase noise around 10^{-1}Hz for the overall clock than for the crystal oscillator. It may be possible to achieve a better shape of Doppler spectrum using crystal oscillators than with atomic clocks in some circumstances, alleviating all of the types of degradation described in Section 3 apart from frequency drift. Specifications of the output of the 5071A after filtering with a crystal oscillator given in Microsemi (2014, 2) show a value of $\mathcal{L}(f)$ at 0.1Hz about 25dB lower than the value predicted by the model in Section 5.

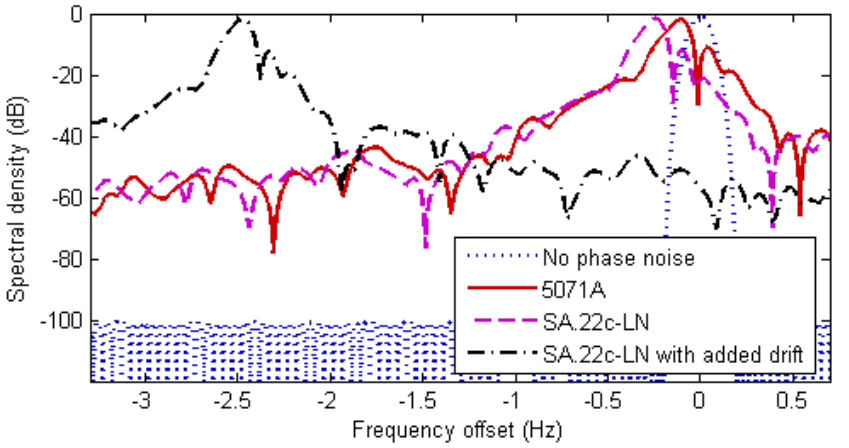

FIGURE 7. Comparison of Caesium and Rubidium clocks at 20GHz and 20s.

7. Conclusions

Close to carrier phase noise can be problematic in bistatic radar systems, particularly for applications with high carrier frequencies and integration times, as there is no correlation between the frequency sources on the transmit and receive platforms. The problems can be alleviated to some extent by the use of atomic clocks, which are more stable than crystal oscillators at lower frequencies.

This paper has described a method of modelling the phase noise in a caesium clock by combining two standard power law models. The values of the model coefficients were estimated using the clock specifications and measured data. The effects of the modelled phase noise on radar performance have been illustrated. The modelling approach has also been applied to rubidium clocks. However, rubidium clocks are more susceptible to environmental and long term non-random effects than caesium clocks and the modelling approach may be less effective. The model could also be applied with different types of clock on the transmit and receive platforms. This type of model could be incorporated into a more general model of a radar system in order to provide estimates of the effects of clock induced phase noise at arbitrary frequencies and integration time.

REFERENCES

ALLAN, D. W. 1987. Time and Frequency (Time-Domain) Characterization, Estimation, and Prediction of Precision Clocks and Oscillators, *IEEE Transactions on Ultrasonics, Ferroelectrics and Frequency Control* **UFFC-34**, **6**, 647-654.

ALLAN, D. W., ASHBY, N. & HODGE, C. C. 1997. The Science of Timekeeping, *Hewlett Packard Application Note* **1289**.

AUDOIN, C. & VANIER, J. 1976. Atomic frequency standards and clocks, *Journal of Physics E: Scientific Instruments* **9**, **9**, 697-720.

BAUCH, A. 2003. Caesium atomic clocks: function, performance and applications, Measurement science and technology, **14**, **8**, 1159-1173.

BELCHER, M. L. & MORRIS, G. V. 1993. Pulsed Doppler Radar, *Coherent Radar Performance Estimation*, edited by SCHEER, J. A. & KURTZ, J. L., Artech House, chapter 9.

CUTLER, L. S. & SEARLE, C. L. 1966. Some Aspects of the Theory and Measurement of Frequency Fluctuations in Frequency Standards, *Proceedings of the IEEE* **54, 2**, 136-154.

CHORTI, A. & BROOKES, M. 2006. A Spectral Model for RF Oscillators with Power-law Phase Noise, *IEEE Transactions on Circuits and Systems-I: Regular Papers* **53**, **9**, 1989-1999.

DIEZ, J., D'Angelo, P. & Fernández, A. 2006. Clock Errors Simulation and Characterisation, *Proceedings of the Institute of Navigation – 19th International Technical Meeting of the Satellite Division*, ION GNSS, 815-821.

EWELL, G. W. 1993. Stability and Stable Sources, *Coherent Radar Performance Estimation*, edited by SCHEER, J. A. & KURTZ, J. L., Artech House, chapter 2.

GREENALL, C. A. 1998. Spectral Ambiguity of Allan Variance, *IEEE Transactions on Tnstrumentation and Measurement* **47**, **3**, 623-627.

HORNE, A. M. & Yates, G. 2002. Bistatic synthetic aperture radar, *Proceedings of Radar 2002*, IEE Conference Publication Number 490, 6-10

IEEE STANDARDS COORDINATING COMMITTEE 27. 2009. IEEE Standard Definitions of Physical Quantities for Fundamental Frequency and Time Metrology – Random Instabilities, *IEEE Std* **1139-2008**.

KRIEGER, G. & YOUNIS, M. 2006. Impact of Oscillator Noise in Bistatic and Multistatic SAR, *IEEE Geoscience and Remote Sensing Letters* **3**, **3**, 424-428.

LEWIS, L. L. 1991. An Introduction to Frequency Standards, *Proceedings of the IEEE* **79**, **7**, 927-935.

MICROSEMI 2014, 5071A Primary Frequency Standard, *Microsemi product data sheet*.

MICROSEMI 2014, 2. 4145C Ultra-Clean Phase-Locked Oscillator, *Microsemi product data sheet*.

SHIN, M. Y., PARK, C. & LEE, S. J. 2008. Atomic Clock Error Modelling for GNSS Software Platform, *IEEE/ION Position, Location and Navigation Symposium*, 71-76.

SYMMETRICOM 2012, SA.22c-LN Low Noise Rubidium Oscillator, *Symmetricom product data sheet*.

WILLIS, N. J. 1990. Bistatic Radar, *Radar Handbook*, edited by Skolnik, M. I., McGraw-Hill, second edition, chapter 25.